

# Variable Chandler and Annual Wobbles in Earth's Polar Motion During 1900–2015

Guocheng Wang<sup>1</sup> · Lintao Liu<sup>1</sup> · Xiaoqing Su<sup>2</sup> ·  
Xinghui Liang<sup>1</sup> · Haoming Yan<sup>1</sup> · Yi Tu<sup>3</sup> · Zhonghua Li<sup>1</sup> ·  
Wenping Li<sup>4</sup>

Received: 9 May 2016 / Accepted: 13 September 2016 / Published online: 4 October 2016  
© The Author(s) 2016. This article is published with open access at Springerlink.com

**Abstract** The Chandler wobble (CW) and annual wobble (AW) are the two main components of polar motion, which are difficult to separate because of their very close periods. In the light of Fourier dictionary and basis pursuit method, a Fourier basis pursuit (FBP) spectrum is developed, which can reduce spectral smearing and leakage caused by the finite length of the time series. Further, a band-pass filtering method based on FBP spectrum (FBPBPF), which can effectively suppress the edge effect, is proposed in this paper. The simulation test results show that the FBPBPF method can effectively suppress the edge effect caused by spectral smearing and leakage and that its reconstruction accuracy at the boundary is approximately three times higher than the Fourier transform band-pass filtering method, which is based on Hamming windowed FFT spectrum, in extracting quasi-harmonic signals. The FBPBPF method is then applied to Earth's polar motion data during 1900–2015. Through analyzing the amplitude and period variations of CW and AW, and calculating the eccentricity variation of the AW, we found that: (1) the amplitude of the CW is currently at a historic minimum level, and it is even possible to diminish further until a complete stop; and (2) the eccentricity of the AW has a gradually decreased fluctuation during the last 116 years.

**Keywords** Chandler wobble · Annual wobble · Band-pass filtering · Fourier basis pursuit spectral · Fourier basis pursuit band-pass filtering

---

✉ Lintao Liu  
llt@whigg.ac.cn

<sup>1</sup> State Key Laboratory of Geodesy and Earth's Dynamics, Institute of Geodesy and Geophysics, Chinese Academy of Sciences, CAS, Wuhan 430077, China

<sup>2</sup> Shandong University of Technology, Zibo 255000, China

<sup>3</sup> College of Civil Engineering and Architecture, China Three Gorges University, Yichang 443002, China

<sup>4</sup> Hunan Institute of Technology, Hengyang 421002, China

## 1 Introduction

Earth's axis is moving with respect to its crust which is called Earth's polar motion. This movement covers external torques and internal excitation processes. External torques ascribable to the gravitational attraction of the Sun, Moon, and planets cause the solid body of the Earth to tidally deform, giving rise to changes in the rotation rate of the Earth. Internal excitation processes such as the atmospheric pressure, wind term, ocean, and groundwater also cause the Earth's rate of rotation to change, and lead the Earth to wobble as it rotates (Nastula and Ponte 1999; Gross et al. 2003; Klimov et al. 2014; Zotov and Bizouard 2015). Polar motion is one important measurement index that reflects the variation of Earth's rotation, so the analysis of its composition is of great importance in understanding the dynamic interactions between the solid Earth, atmosphere, oceans, and other geophysical fluids, as well as studying its excitation (Höpfner 2003a, 2004; Malkin and Miller 2010; Smylie et al. 2015). Thus, along with examining the eccentricity variation of the AW, it is meaningful to study the amplitude and period variations of the Chandler wobble (CW) and annual wobble (AW), which are the two main components of polar motion.

Until about 1980, optical astrometry was used to measure the Earth's changing rotation for more than about a century. Currently, several space-geodetic techniques are available, such as VLBI (very-long-baseline radio interferometry), LLR (lunar laser ranging), SLR (satellite laser ranging), GPS (global positioning system), and DORIS (Doppler orbit determination and radio positioning integrated on satellite) (Gross 2000; Höpfner 2003a, 2004; Lambeck 2005).

Four combined Earth orientation parameter (EOP) solutions are released by the International Earth Rotation Service (IERS), namely EOP(IERS) C01 between 1846 and 1890; it has a 0.1-year sampling interval, and after this a 0.05-year interval, EOP (IERS) C02 since 1962 at 5-day intervals, EOP (IERS) C03 since 1993 at 1-day intervals, and EOP(IERS) C04 since 1962 at 1-day intervals (IERS 1999; Höpfner 2003a, 2004). For more information on polar motion time series, see Höpfner (2000, 2004) and references therein. The Earth rotation series used in this study is EOP C01 during 1900–2015.

The secular drift having a rate of about 3.5 mas/year, the Chandler wobble having a variable amplitude ranging between about 100–200 mas, and the annual wobble having a nearly constant amplitude of about 100 mas are three dominant components of polar motion (Gross 2000). In addition, polar motion has the following periods: semi-Chandler, semiannual periods and those of order four, three, two, and one and a half months, as well as quasi-biennial and 300-day periods (Höpfner 2003a).

Since CW was first observed by Chandler in 1891 (Chandler 1891), its component analysis has been extensively researched (Lenhardt and Groten 1985; Wilson and Vicente 1990; Schuh et al. 2001; Jochmann 2003; Höpfner 2003b, 2004; Guo et al. 2005; Liu et al. 2007). Because of the existence of two peaks in its FFT spectrum, some authors consider the CW to be an oscillation with two close frequencies (Guo et al. 2005); however, other authors think of it as time-varying frequencies; these two peaks would be attributed to some unusual phase variation ( $180^\circ$  shift) of the CW during the 1920–1930s (Malkin and Miller 2010). On CW, a number of studies (Okubo 1982; Kuehne et al. 1996; Vicente and Wilson 1997) provided evidence for a constant Chandler period, while others (Melchior 1954, 1957; Sekiguchi 1972, 1976; Carter 1981) suggested a time-varying period which varies between 1.13 and 1.20 years (413 and 439 days) (Schuh et al. 2001).

The CW is an excited resonance of the Earth's rotation but, as the Earth is a viscous–elastic body, it would freely decay with a time constant of about 68 years to the minimum rotational energy state of rotation about the figure axis in the absence of excitation (Gross 2000; Gross et al. 2003; Lambeck 2005). Although CW has been under investigation for more than a century, its excitation mechanism has remained elusive (Lenhardt and Groten 1985; King and Agnew 1991; Gross 2000; Höpfner 2004; Malkin and Miller 2010). Up to now, various hypotheses on CW excitation have been proposed, such as atmospheric and oceanic processes (Brzeziński et al. 2002, 2012; Bizouard et al. 2011; Brzeziński and Nastula 2002; Salstein 2000; Gross et al. 2003; Zotov and Bizouard 2015), wind and surface pressure variations (Wahr 1982; Gross et al. 2003), groundwater impulses, changes in snow cover, interaction at the boundary between the core and mantle, and earthquakes (Dahlen 1971, 1973; Höpfner 2004; Smylie et al. 2015).

The AW is a forced motion and can be written as a sum of prograde and retrograde parts, and the prograde part is about ten times larger than the retrograde part (King and Agnew 1991). The prograde part of AW has a significant change in the period ranging between 356 and 376 days (Höpfner 2004). The excitation of the AW has been a hot topic. Chao and O'Connor (1988) studied the hydrologic contributions to the annual wobble and found that the land water contribution is far smaller than previously estimated when combining the rainfall and snow load contributions from satellite data. Kuehne and Wilson (1991) studied the groundwater contribution using their 612 basin global model forced by monthly mean precipitation estimates and concluded that its amplitude is only about 10 % of the atmospheric contribution in the prograde AW. Using meteorological data available at different time spans, some authors calculated the atmospheric excitation of the AW in terms of the polar motion excitation function and showed that atmospheric angular momentum (AAM) changes are a primary cause for the Earth's AW (Munk 1961; Wilson and Haubrich 1976; Daillet 1981; Merriam 1982; Wahr 1982; Chao and Au 1991). Zhong (2003) made an investigation of atmospheric, hydrologic, and ocean current contributions to seasonal polar motion based on a coupled ocean–atmosphere general circulation model and confirmed the importance of hydrology as a source of the AW. Gross et al. (2003) compared the contributions to the annual wobble such as atmospheric, wind, surface pressure, oceanic and currents and found that the effects of winds and currents on exciting the annual wobble have nearly the same retrograde amplitude and a prograde amplitude that differs by about 30 %, and the effect of currents on exciting the annual wobble is about 2/3 of the effect of bottom pressure variations. Höpfner (2004) considered the excitations of the AW to come from the seasonal displacement of air and water masses.

The CW is one of the main eigenmodes of the Earth rotation, and investigation of its properties such as period, amplitude, and phase variations are very important for the understanding of the physical processes in the Earth, including its surface, interior, atmosphere, and ocean (Malkin and Miller 2010). The amplitude, period, and phase properties of AW extracted from the observed polar motion are very important for studying the excitation mechanism of AW. However, the frequencies of the CW and the prograde annual wobble (PAW) are too close, and their amplitudes are both great, so the energy of these terms produces interaction effects, and as a result the CW and AW are difficult to separate.

In order to separate the CW and AW from the polar motion time series and study their behaviors over time, band-pass filters have often been employed. For example, a Fourier transform band pass filter (FTBPF) with cosine-bell transfer function was applied both for polar motion analysis and extracting the CW and AW from IERS93C01 pole coordinate data and IERS90C04 pole coordinates data, respectively (Popiński and Kosek 1995; Kosek

1995). Wavelet transform was used to determine and analyze the periods and amplitudes of the CW and AW (Schuh et al. 2001). Zero-phase digital filters were applied to filter out the CW and AW from several homogeneous PM time series, distinguished by a variety of sampling intervals the polar motion time series, such as POLE2001 (JPL), EOP (IERS) C01, OA00 (AICAS), EOP (IERS) C04, and SPACE2001 (JPL) (Höpfner 2004). Furthermore, in recent years, Malkin and Miller (2010) applied the singular spectrum analysis (SSA) and Fourier transform to extract the CW and then examined the CW amplitude and phase variations by means of the wavelet transform and Hilbert transform, their analysis had shown that besides the well-known CW phase jump in the 1920s, two other large phase jumps have been found in the 1850s and 2000s, and as in the 1920s, these phase jumps occurred with a sharp decrease in the CW in the 2000s; Zotov and Bizouard (2015) utilized the time domain excitation in Chandler frequency band which was extracted by Pantelev's filtering method to investigate the evolution of the regional atmospheric influence on CW; Smylie et al. (2015) applied the maximum entropy method (MEM) to remove the AW, and leaving a pure CW and secular polar shift; hence, it overcomes the usual problem of how to avoid mixing the AW and CW which is beneficial to reveal details of the effect of earthquakes on the polar motion. However, because of the edge effect present in all of the above methods, a few of the estimates at the beginning and end of the time series may be less accurate, and the closer to the edge point, the less accurate the estimates would appear to be. The accurate determination of boundary value in a short time is necessary in the study on the amplitude, phase, and period of the CW and AW, and accurate information of the boundary is also necessary for the prediction of polar motion.

In order to suppress the edge effect, we developed a Fourier basis pursuit (FBP) spectrum and a Fourier basis pursuit band-pass filtering (FBPBPF) method in this paper. Based on the amplitude, period, and phase features of the CW and PAW, a synthetic polar motion time series was simulated. The FTBPF methods and the FBPBPF method are carried out to separate and reconstruct the simulated CW and AW. The FTBPF methods adopt two kinds of FFT spectrum with the boxcar window and the Hamming window in this paper. The reconstruction accuracy using FBPBPF and FTBPF methods at the boundary is evaluated; simulation experiment results show the reconstruction accuracy of the CW and AW using the FTBPF method, where the FFT spectrum with Hamming window is much higher than the one with boxcar window. The FBPBPF method is superior to FTBPF method; the reconstruction accuracy of the former is approximately three times higher than that of the latter which is based on the FFT spectrum with Hamming window at the boundary. Moreover, there is no obvious increase in the residual error at both time series ends using the FBPBPF method to extract the CW and AW from the EOP (IERS) C01 series. These results show that the FBPBPF method can effectively inhibit the edge effect, relative to the aforementioned FTBPF methods. Moving forward, the period variations, the amplitude variation of the CW and AW, and the eccentricity variation of the AW at the boundary extracted from the EOP (IERS) C01 series via the FBPBPF method are considered to be reliable.

The structure of this paper is as follows. The FTBPF with two types of windows and FBPBPF methods are introduced, respectively, and the reconstruction accuracies of the simulation CW and AW are compared using these two filtering methods in the second section. In the third section, the FBPBPF method is used to extract the CW and AW from the EOP (IERS) C01 series during the time period from 1900 to 2015. The amplitude and period of the CW and AW and the eccentricity of the AW are also analyzed, and we summarize results in the fourth section.

## 2 Band-Pass Filtering Methods and Their Comparisons

### 2.1 Fourier transform band pass filter (FTBPF)

Fourier transform (FT) is one of the most basic of mathematical transformations and also is an effective tool to analyze the frequency characteristics of the signal. Its application is extensive; the FTBPF has already been used to extract the CW and AW from the polar motion signal (Popiński and Kosek 1995; Kosek 1995; Schuh et al. 2001).

For a time signal  $f(j)$ , its discrete Fourier transform (DFT) is obtained as follows:

$$F(k) = \sum_{j=1}^N f(j) \exp(-2\pi i(j-1)(k-1)/N) \quad (1)$$

where  $k = 1, 2, \dots, N$ ,  $N$  is the length of the data, the  $k$  value corresponds to the angular frequency value  $\omega_k$ .

Referring to the finite length of time series, it is often related to spectral leakage when using DFT. Window functions are used in harmonic analysis to reduce the undesirable effects related to spectral leakage (Harris 1978). Then, the DFT with window is obtained as follows.

$$F_w(k) = \sum_{j=1}^N f(j)w(j) \exp(-2\pi i(j-1)(k-1)/N) \quad (2)$$

where  $F_w(k)$  is the DFT with window function,  $w(j)$  is the window function. The formula (1) is equivalent to adding boxcar window for the time series  $f(j)$ . The Hamming window was also used in this paper. These two types of windows are shown in formulas (3) and (4), respectively.

The definition of the boxcar window is as follow.

$$w(j) = 1, j = 1, 2, \dots, N \quad (3)$$

where  $N$  is the length of the time series to analyze.

The definition of the Hamming window is as follow.

$$w(j) = \begin{cases} 0.54 + 0.46 \cos\left(\frac{2\pi}{N}(j - N/2)\right), & j = 1, 2, \dots, N/2 \\ 0.54 - 0.46 \cos\left(\frac{2\pi}{N}(j - N/2)\right), & j = N/2 + 1, \dots, N \end{cases} \quad (4)$$

where  $N$  is the length of the time series to analyze.

For the discrete form of signal  $f(j)$ , its DWT with window can be inverted through:

$$f(j) = \sum_{k=1}^N F(k) \exp(2\pi i(j-1)(k-1)/N)/w(j)/N \quad (5)$$

Here,  $j = 1, 2, \dots, N$ . More information on window functions can be seen in Harris (1978) and references therein.

If the  $k$  value takes the corresponding angular frequency range  $[\varpi_1, \varpi_2]$ , then the value obtained with the FTBPF is:

$$z(j) = \sum_{k=K_{\varpi_1}}^{K_{\varpi_2}} F(k) \exp(2\pi i(j-1)(k-1)/N)/w(j)/N \quad (6)$$

where  $K_{\varpi_1}$  corresponds to the frequency value  $\varpi_1$ ,  $K_{\varpi_2}$  corresponds to the frequency value  $\varpi_2$ . Here, the frequencies  $\varpi_1$  and  $\varpi_2$  and corresponding integers  $K_{\varpi_1}$  and  $K_{\varpi_2}$  cannot be arbitrary. The difference  $\varpi_2 - \varpi_1$  should be greater than the minimum frequency resolution, which mostly depends on the number of data  $N$  when using DFT.

## 2.2 Fourier basis pursuit band pass filter (FBPBPF)

Sparse representations of signals have received a great deal of attention in recent years (Elad et al. 2006a; Huang and Aviyente 2006; Rubinstein et al. 2010). Using an overcomplete dictionary that contains prototype signal-atoms, signals are described by sparse representations of these atoms. Research has focused on three aspects of the sparse representation: (1) pursuit methods for solving the optimization problem, such as matching pursuit (Mallat and Zhang 1993), the method of frames (Daubechies 1988), orthogonal matching pursuit (Pati et al. 1993), basis pursuit (Chen et al. 1998), and Least Angle Regression (LARS) is a useful and less greedy version of traditional forward selection methods. LARS closely parallels the homotopy method. LARS/homotopy methods are used for optimization (Drori and Donoho 2006). Among these pursuit methods, the results obtained by basis pursuit method are the most sparse (Chen et al. 1998; Mallat 1999); (2) choosing a given dictionary, such as the Fourier dictionary, Dirac dictionary, Heaviside dictionary, cosine packet (Coifman and Mayer 1991), wavelet dictionary, chirplet dictionary (Mihovilović and Bracewell 1991; Mann and Haykin 1992), warplets dictionary (Baraniuk and Jones 1993), or designing of the dictionary, such as the K-SVD method (Elad et al. 2006a). Among these given dictionaries, the Fourier dictionary, which is suitable for the analysis and extraction of quasi-harmonic signals or harmonic signal, is the most widely used dictionary; (3) the applications of sparse representation for different tasks, such as signal separation, denoising, coding, and image inpainting (Olshausen et al. 2001; Starck et al. 2005; Li et al. 2004; Elad and Aharon 2006; Elad et al. 2006b).

The spectrum using basis pursuit can achieve a higher spectral resolution because it can efficiently reduce spectral smearing and leakage caused by the finite size of the time series (Tary et al. 2014). So the basic principle of the FBP spectrum and the FBPBPF method, which are based on the Fourier dictionary and basis pursuit, are developed in this paper. Through global optimization, the FBP spectrum can achieve the optimal allocation of amplitude at a fixed frequency. Then, the FBPBPF method can effectively identify and separate the coupled signal, which consists of two or more quasi-harmonic signals. The CW and AW in the polar motion signal are quasi-harmonic signals, whose frequencies are close to each other, so it is fitting to extract these two terms using the FBPBPF method.

Based on the formula (5), in which  $\omega(j)$  is the boxcar window, the matrix  $\Phi$  is established:

$$\Phi = \begin{bmatrix} \exp(2\pi i \times 0 \times J/N)/N \\ \exp(2\pi i \times 1 \times J/N)/N \\ \vdots \\ \exp(2\pi i \times (N-1) \times J/N)/N \end{bmatrix}_{N \times M} \quad (7)$$

where  $J = [0, 1, \dots, M-1]$ .  $M$  is the number of atoms in the dictionary,  $N$  is the length of the time series. Each column of the matrix  $\Phi$  represents the atomic of the Fourier dictionary. The dictionary is overcomplete for  $M > N$ , in which case the number of atoms is

greater than the length of the time series (Chen et al. 1998). Each atom of the Fourier dictionary demonstrates different frequency characteristics. Thus, formula (5) is written in the form  $\Phi x = f$ , in which  $f$  is the original signal and  $x$  is the corresponding coefficient of the Fourier dictionary.

The principle of basis pursuit is to find a representation of the signal whose coefficients have minimum  $l_1$  norm (Mallat 1999). Formally, one solves the problem if

$$x^* = \arg \min_{x \in R^p} \|x\|_1 \quad \text{subject to } \Phi x = f \quad (8)$$

The basis pursuit minimization of formula (8) is a convex optimization that can be reformulated as a linear programming problem (Mallat 1999). Over the last 50 years, a tremendous amount of work has been done on the solution of linear programs, and some spectacular breakthroughs have been made through the use of the so-called interior point methods (Chen and Donoho 1994).

Through global optimization, basis pursuit can obtain a better resolution than matching pursuit and can get a better result than the method of frames (Chen and Donoho 1994; Chen et al. 1998).

The matrix  $\Phi$  is the Fourier dictionary, and the solution  $x^*$  of the formula (8) obtained according to  $l_1$  norm, then the solution  $x^*$  can be defined as the FBP spectrum. If  $x^*$  takes the corresponding angular frequency range  $[\varpi_1, \varpi_2]$ , the corresponding filtering results are obtained, and the FBPBPF method can be defined as

$$z = \Phi x^* \quad (9)$$

where, in formula (9),  $z$  is the corresponding filtering results with angular frequency range  $[\varpi_1, \varpi_2]$ . Here, the difference  $\varpi_2 - \varpi_1$  should be greater than the minimum frequency resolution which mostly depends on fixed frequency interval.

### 2.3 Simulation and Comparison Results

In order to compare the reconstruction accuracy of these two filtering methods, we simulate the polar motion time series which contained the model CW and PAW oscillations. The amplitude of the model CW is 200, and the period is 435; the amplitude of the model PAW is 100, and the period is 365. The model time series have a 20/365 sampling interval. For some studies considering that unusual phase variation ( $180^\circ$  shift) exists in the CW (Malkin and Miller 2010), we added the phase variation in the simulation polar motion time series (as shown in Fig. 1).

$$f(t) = \begin{cases} 200 \left( 1 + 0.2 \cos \left( \frac{2\pi t}{10000} \right) \right) \exp \left( \frac{i \times 2\pi t}{435} \right) \exp \left( -\frac{t}{60000} \right) + 100 \left( 1 + 0.2 \cos \left( \frac{2\pi t}{12500} \right) \right) \exp \left( \frac{i \times 2\pi t}{365} \right) \exp \left( \frac{t}{100000} \right) + \varepsilon(t) & 1 \leq t < 400 \\ 200 \left( 1 + 0.2 \cos \left( \frac{2\pi t}{10000} \right) \right) \exp \left( \frac{i \times 2\pi t}{435} + \pi \right) \exp \left( -\frac{t}{60000} \right) + 100 \left( 1 + 0.2 \cos \left( \frac{2\pi t}{12500} \right) \right) \exp \left( \frac{i \times 2\pi t}{365} \right) \exp \left( \frac{t}{100000} \right) + \varepsilon(t) & 400 \leq t \leq 2000 \end{cases} \quad (10)$$

where  $\varepsilon$  is white noise, and its mean value and variance are 0 and 10, respectively.

As shown in Fig. 2, the peaks shown in the FBP spectrum are far higher than those shown in the FFT spectrum; Fig. 2 certainly demonstrates that the FBP spectrum is more efficient in reducing spectral smearing than the FFT spectrum. It should be noted that the small peaks shown in the FBP spectrum can be considered as the spectrum leakage, because the modeled time series are quasi-harmonic signals, rather than harmonic signals, so their FBP spectrum should be represented by not only several big peaks, but also some



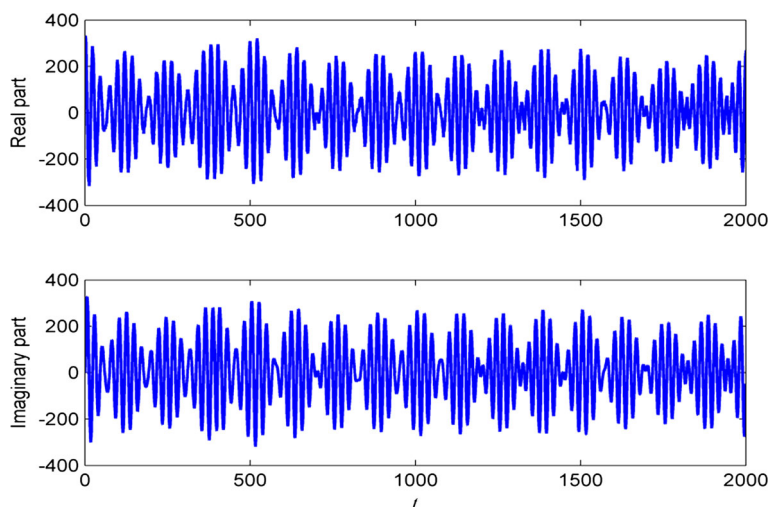


**Fig. 1** Modeled time series. The real part of modeled time series can be shown in (*top*); the imaginary part can be shown in (*bottom*)

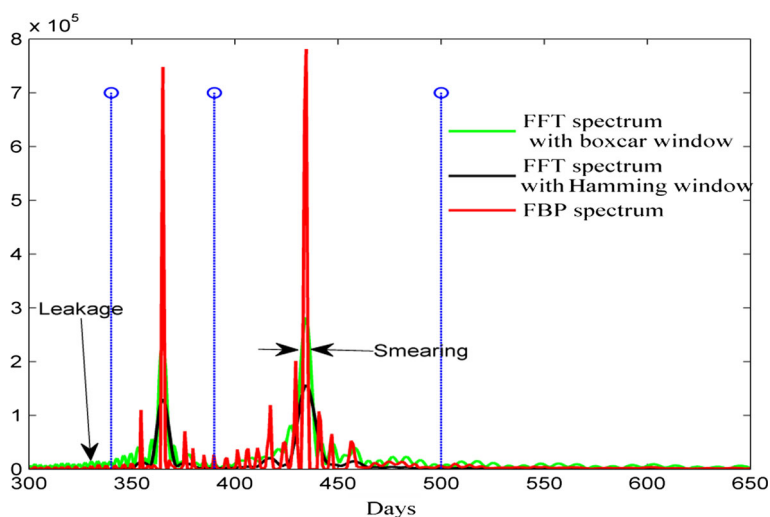


**Fig. 2** FFT spectrum and FBP spectrum. The *blue lines* are, in order, 340, 390, and 500

small peaks; however, these spectrum leakage is convergent in a limited range, while the spectrum leakage of FFT spectrum with boxcar window is in a wider range. The FBP spectrum and FFT spectrum with Hamming window can both effectively reduce spectrum leakage with respect to the FFT spectrum with boxcar window.

Then, in order to extract the modeled CW and PAW as full as possible, a wider periodic range is selected, as shown in Fig. 2; the corresponding range of the modeled CW and PAW in FFT spectrum and FBP spectrum is 340–390, and 390–500, respectively.

The modeled CW and PAW extracting from the model polar motion time series using these above methods are shown in Figs. 3, 4, and 5.



Comparison Figs. 3, 4, and 5, the usage of FBPBPF method is highest. However, to some degree, these band-pass filtering results all involved a loss of precision at the phase variation point. The reconstruction precision at the boundary is very important. The comparison of the reconstruction precision of 100 values at the right boundary using those methods is shown in Tables 1 and 2.

As shown in Tables 1 and 2, whether from the perspective that the root-mean-square error or the point of the maximum value of absolute error at the boundary, the reconstruction precision using the FBPBPF method is highest and the reconstruction precision using the FBPBPF method is approximately three times higher than using the FTBPF method with Hamming window. The FTBPF method with Hamming window can improve the reconstruction precision relative to that of the boxcar window. Therefore, we can say that the FBPBPF method can more effectively suppress the edge effect than the FTBPF methods with these two types of windows. The results of Fig. 2, Tables 1 and 2 show that the FBP spectrum can more reduce spectral smearing and leakage, and the FBPBPF method can more effectively suppress the edge effect.

### 3 Variable Chandler and Annual Wobbles During 1900–2015

In order to analyze the characteristics of the amplitude variation and period variation of the CW and AW in Earth's polar motion, we used the EOP (IERS) C01 series during 1900–2015, published by the International Earth Rotation and Reference System Service (IERS) (as seen in Fig. 6). The EOP (IERS) C01 series have a 0.05-year sampling interval.

After removing the linear trends of the polar motion series using the least square method, we can obtain the FBP spectrum (seen in Fig. 7).

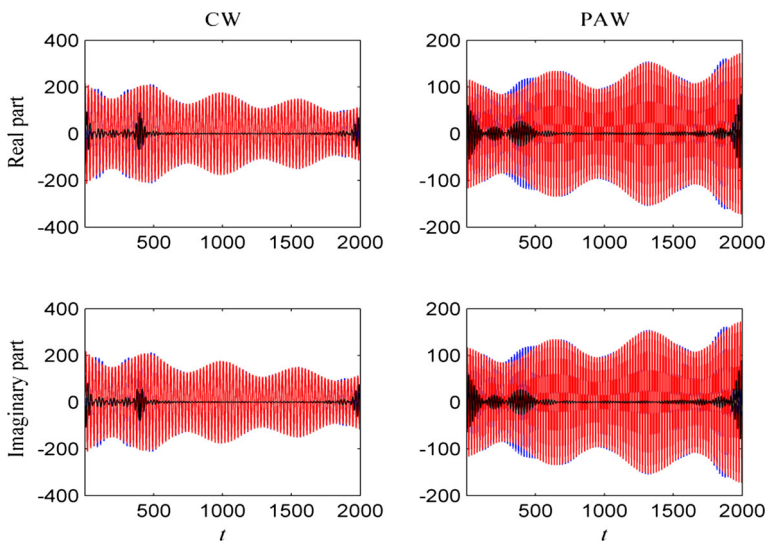


**Fig. 3** Reconstruction results using the FTBPF method with boxcar window (*red* for the simulation signal, *blue* for the reconstruction of the signal, *black* for the reconstruction error)

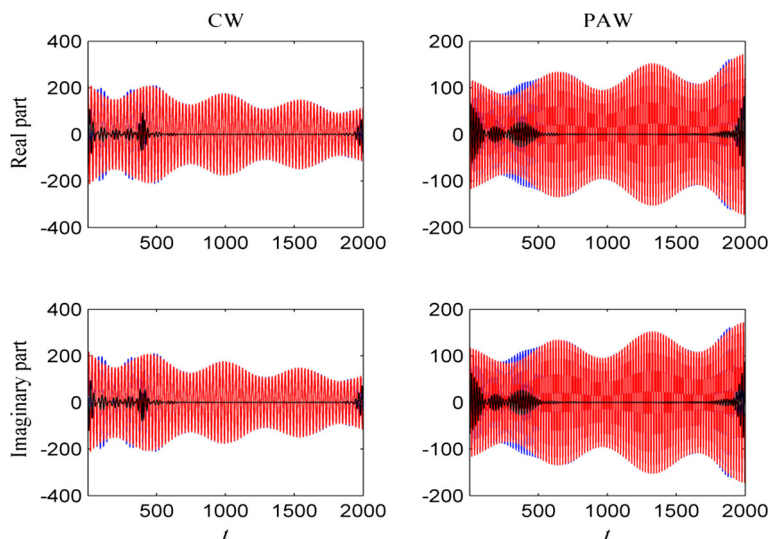


**Fig. 4** Reconstruction results using the FTBPF method with Hamming window (*red* for the simulation signal, *blue* for the reconstruction of the signal, *black* for the reconstruction error)

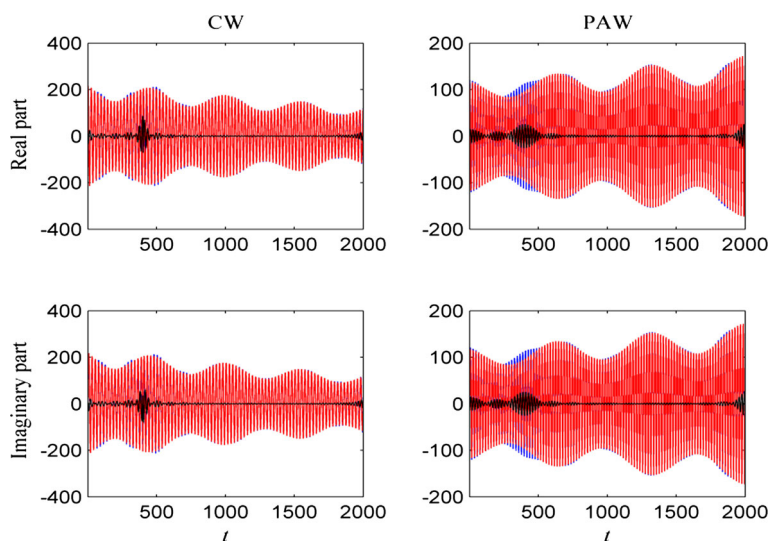


**Fig. 5** Reconstruction results using the FBPBPF method (*red* for the simulation signal, *blue* for the reconstruction of the signal, *black* for the reconstruction error)

As shown in Fig. 7, a wider periodic range of the CW, PAW, and Retrograde Annual wobble (RAW) is selected in FBP spectrum in order to reduce the spectral leakage. The reconstruction was carried out in accordance with formula (7), and the CW, PAW, and RAW obtained, respectively, as shown in Figs. 8, 9, and 10.

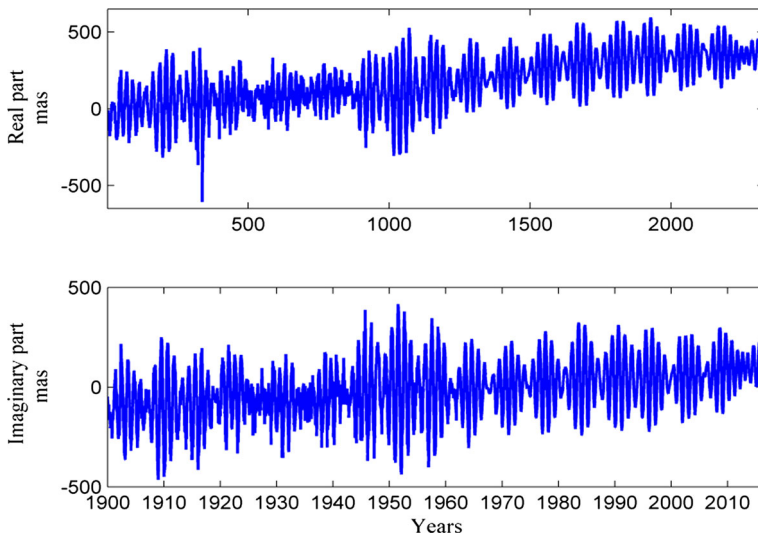
After removing the linear trend term, the CW, PAW, and RAW from the polar motion series, the residual time series were obtained (Fig. 11).

**Table 1** RMS with different filtering methods at the boundary

	FTBPF with boxcar window	FTBPF with Hamming window	FBPBPF
The real part of simulation CW	57.05	28.56	7.89
The imaginary part of simulation CW	55.23	26.30	8.28
The real part of simulation PAW	100.45	32.88	11.09
The imaginary part of simulation PAW	99.67	34.06	11.20

**Table 2** The maximum value of absolute error with different methods at the boundary

	FTBPF with boxcar window	FTBPF with Hamming window	FBPBPF
The real part of simulation CW	107.66	78.20	18.36
The imaginary part of simulation CW	106.57	70.97	19.49
The real part of simulation PAW	156.86	80.97	27.34
The imaginary part of simulation PAW	156.10	87.06	27.11

**Fig. 6** Polar motion (PMx, PMy) observations time from 1900 to 2015

As shown in Fig. 11, there is no obvious edge effect, that is, the residual value at the both ends of the residuals is not significantly increased in relation to the middle. This shows that the FBPBPF method can effectively suppress the edge effect. Moreover, there is an apparent peak value in the residual time series during the 1920–1930s, which may have been caused by the unusual phase variation of the CW during the 1920–1930s (Malkin and Miller 2010). This result is in accordance with the simulation.

The complex-valued polar motion time series can be expressed as:

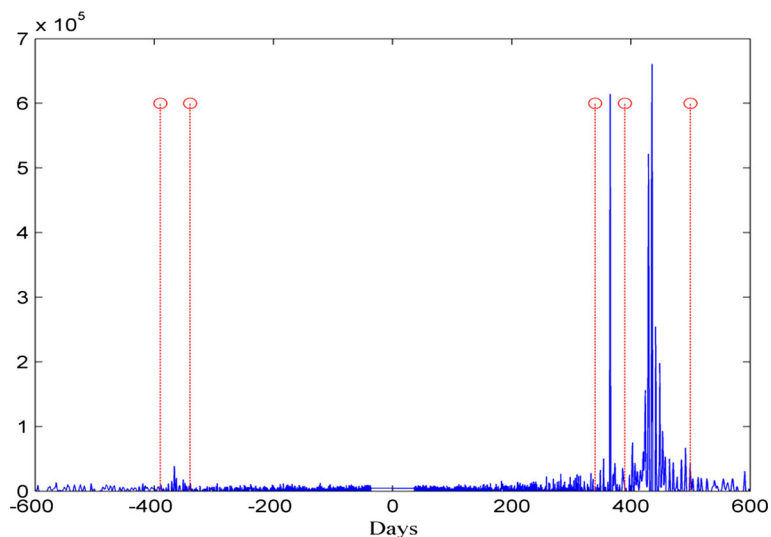


**Fig. 7** FBP spectrum. The red dash lines are, in order,  $-390$ ,  $-340$ ,  $340$ ,  $390$ , and  $500$

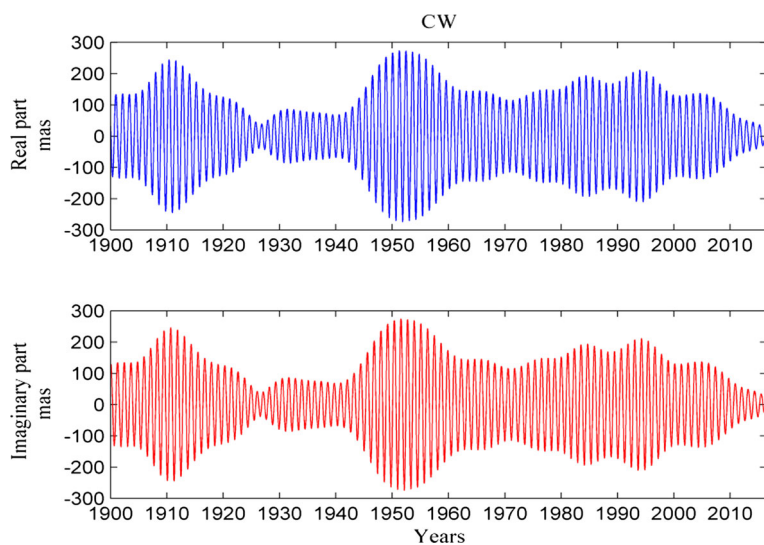


**Fig. 8** Reconstruction of the CW using the FBPBPF method

$$z(t) = x(t) + iy(t) \quad (11)$$

where  $x$  and  $y$  are pole coordinates data.

Then, the amplitude of polar motion is expressed as:

$$r(t) = |z(t)| = |x(t) + iy(t)| = (x(t)^2 + y(t)^2)^{1/2} \quad (12)$$

The complex-valued polar motion time series can be expressed as:

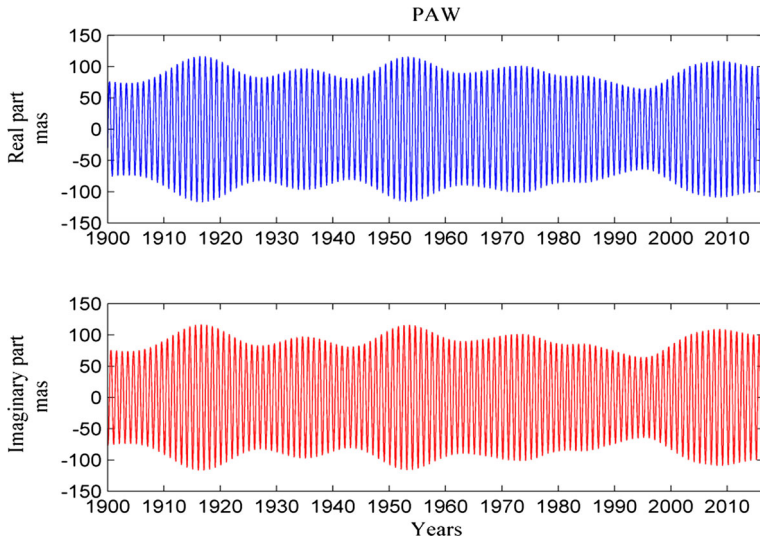


**Fig. 9** Reconstruction of the PAW using the FBPBPF method

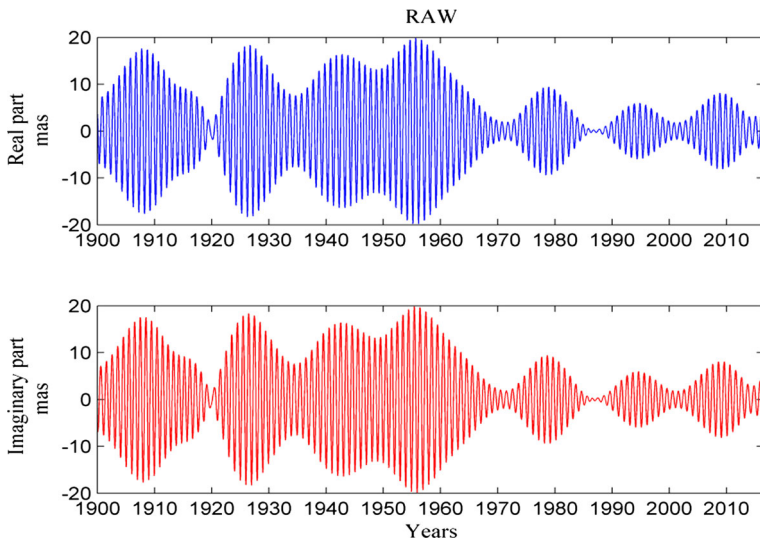


**Fig. 10** Reconstruction of the RAW using the FBPBPF method

$$z(t) = r(t) \exp(i\theta(t)) \quad (13)$$

where  $\theta$  is the phase angle expressed as:

$$\theta(t) = 2\pi\gamma(t)t \quad (14)$$

where instantaneous frequency  $\gamma$  can be expressed as:

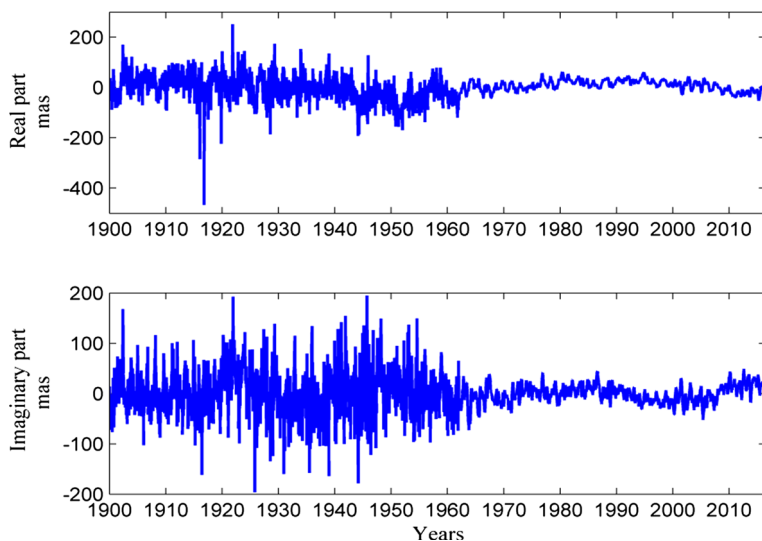


**Fig. 11** Residual time series obtained by the FBPBPF method

$$\gamma(t) = \frac{\dot{\theta}(t)}{2\pi} \quad (15)$$

where  $\dot{\theta}$  is the first-order derivative of phase angle  $\theta$ .

Then, the instantaneous period of polar motion can be expressed as:

$$T(t) = \frac{1}{\gamma(t)} \quad (16)$$

Using formulae (12)–(16), the amplitude variation and instantaneous period variation of the CW, PAW, and RAW can be obtained, shown in Figs. 12 and 13.

As shown in Fig. 12, the amplitude of the CW varies from 43 to 287 mas, which has been diminishing since 1995 and is tending to reduce further. The amplitude of the CW currently is at a minimum level in history, and if the amplitude of the CW is reducing in accordance with this trend, it may diminish in about 2022. The amplitude of the PAW varies from 65 to 118 mas, which has been diminishing since 2010 and has a reducing trend further. The amplitude of the RAW varies from 0.5 to 20 mas. Regarding the amplitude of the RAW, it is generally smaller after 1964 than before; this conclusion is same as King and Agnew result (1991). Moreover, the amplitude of RAW has reached the minimum value point and will soon begin to increase.

As is shown in Fig. 13, the instantaneous periods of CW and PAW vary over the ranges 392–441 days, 359–370 days, respectively. The period of PAW has been oscillating since 1960. The RAW oscillation period has an abnormal value before 1920 year which needs further study, and for other time, its variation range is from –409 to –346 days.

The formula of eccentricity can be expressed as follows:

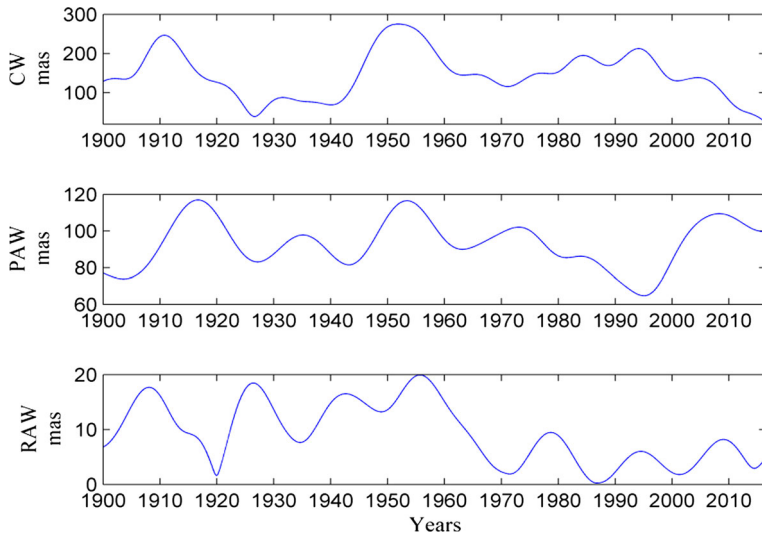


**Fig. 12** Amplitudes of the CW, PAW, and RAW

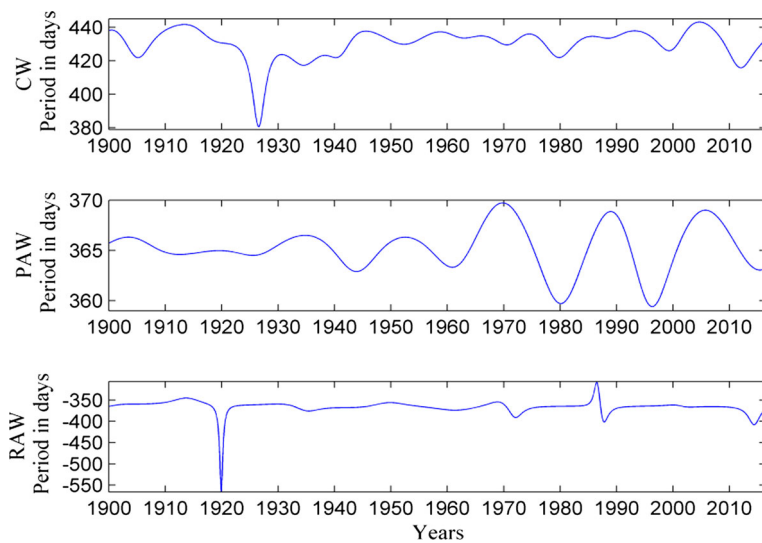


**Fig. 13** Instantaneous periods of the CW, PAW, and RAW

$$e(t) = \frac{\sqrt{a(t)^2 - b(t)^2}}{a(t)} \quad (17)$$

where  $a(t) = \frac{r_{\text{pan}}(t) + r_{\text{ran}}(t)}{2}$ ,  $b(t) = \frac{r_{\text{pan}}(t) - r_{\text{ran}}(t)}{2}$ ,  $r_{\text{pan}}$  and  $r_{\text{ran}}$  denote the amplitude of PAW and RAW, respectively.



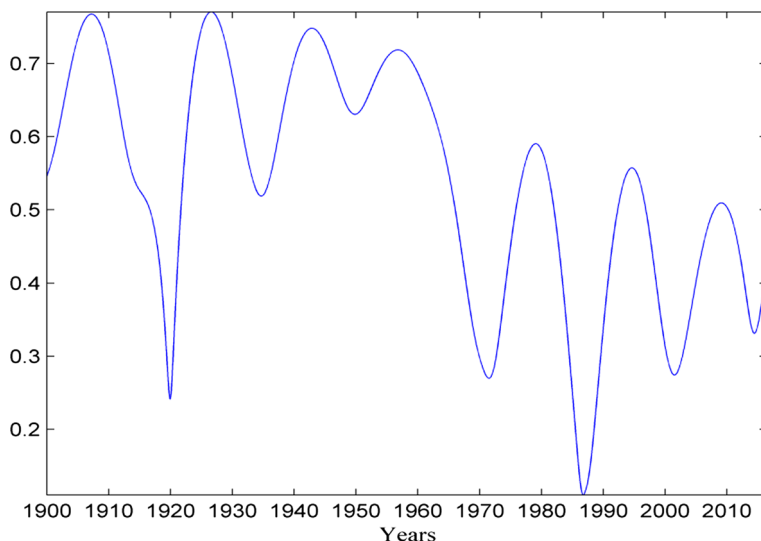


**Fig. 14** Eccentricity of the AW

The eccentricity of AW is shown in Fig. 14.

As shown in Fig. 14, the eccentricity of the AW changes from 0.15 to 0.8 which reached the minimum value in 1986.

## 4 Conclusions

In order to study the variability of the CW and AW of polar motion, the FBPBPF method developed in this paper is applied to extract the CW and AW from the EOP (IERS) C01 series in the time period spanning from 1900 to 2015. This method can effectively suppress the edge effect in band-pass filtering because the FBP spectrum can effectively reduce spectral smearing and leakage and which is proved by a simulated test.

Through analyzing the amplitude and period variations of CW and AW, and the eccentricity variation of the AW, we find that the CW shows significant variations in both amplitude and period, while the AW shows significant variations in amplitude. Particularly, the RAW has relatively large variations in amplitude, and the eccentricity of the AW has decreased (with fluctuation) during the past 115 years, while the PAW has been oscillating in period since 1960.

Finally, it should be noted that the amplitude of the CW has been diminishing since 1995 and currently is at a minimum level in history; however, what is the cause of this phenomenon and what time would it stop the reducing trend? These problems are worth further study.

**Acknowledgments** We are grateful to the International Earth Rotation and Reference Systems Service (IERS) for providing the polar motion data. This study is supported by NSFC 41074050 and by 2011YQ120045 of Ministry of Science and Technology of the People's Republic of China. Also the two anonymous reviewers are thanked for their remarks and suggestions which were helpful in preparing the revised version.

**Open Access** This article is distributed under the terms of the Creative Commons Attribution 4.0 International License (<http://creativecommons.org/licenses/by/4.0/>), which permits unrestricted use, distribution, and reproduction in any medium, provided you give appropriate credit to the original author(s) and the source, provide a link to the Creative Commons license, and indicate if changes were made.

## References

- Baraniuk RG, Jones DL (1993) Shear madness: new orthonormal bases and frames using chirp functions. *IEEE Trans Signal Process* 41(12):3543–3549
- Bizouard C, Remus F, Lambert SB, Seoane L, Gambis D (2011) The Earth's variable Chandler wobble. *Astron Astrophys* 526:A106
- Brzeziński A, Nastula J (2002) Oceanic excitation of the Chandler wobble. *Adv Space Res* 30(2):195–200
- Brzeziński A, Bizouard C, Petrov SD (2002) Influence of the atmosphere on Earth rotation: what new can be learned from the recent atmospheric angular momentum estimates? *Surv Geophys* 23(1):33–69
- Brzeziński A, Dobslaw H, Dill R, Thomas M (2012) Geophysical excitation of the Chandler wobble revisited. In: Kenyon S, Pacino MC, Marti Urs (eds) *Geodesy for planet Earth*. Springer, Berlin, pp 499–505
- Carter WE (1981) Frequency modulation of the Chandlerian component of polar motion. *J Geophys Res Solid Earth* 86(B3):1653–1658
- Chandler SC (1891) On the variation of latitude, I. *Astron J* 11:59–61
- Chao BF, Au AY (1991) Atmospheric excitation of the Earth's annual wobble: 1980–1988. *J Geophys Res Solid Earth* 96(B4):6577–6582
- Chao BF, O'Connor WP (1988) Global surface-water-induced seasonal variations in the Earth's rotation and gravitational field. *Geophys J Int* 94(2):263–270
- Chen S, Donoho D (1994) Basis pursuit. In: *Signals, systems and computers, 1994. 1994 conference record of the twenty-eighth Asilomar Conference*, vol 1, pp 41–44
- Chen SS, Donoho DL, Saunders MA (1998) Atomic decomposition by basis pursuit. *SIAM J Sci Comput* 20(1):33–61
- Coifman RR, Meyer Y (1991) Remarques sur l'analyse de Fourier à fenêtre. *C r de l'Acad des Sci Sér 1 Math* 312(3):259–261
- Dahlen FA (1971) The excitation of the Chandler wobble by earthquakes. *Geophys J Int* 25(1–3):157–206
- Dahlen FA (1973) A correction to the excitation of the Chandler wobble by earthquakes. *Geophys J Roy Astron Soc* 32(2):203–217
- Daillet S (1981) Atmospheric excitation of the annual wobble. *Geophys J Roy Astron Soc* 64(2):373–380
- Daubechies I (1988) Time-frequency localization operators: a geometric phase space approach. *IEEE Trans Inf Theory* 34(4):605–612
- Drori I, Donoho DL (2006) Solution of  $l_1$  minimization problems by LARS/homotopy methods. In: *acoustics, speech and signal processing, 2006. ICASSP 2006 Proceedings. 2006 IEEE International Conference*, vol 3, pp III
- Elad M, Aharon M (2006) Image denoising via learned dictionaries and sparse representation. In: *IEEE computer society conference on computer vision and pattern recognition*, vol 1, pp 895–900
- Elad M, Aharon M, Bruckstein AM (2006a) The K-SVD: an algorithm for designing of overcomplete dictionaries for sparse representations. *IEEE Trans Image Process* 15(12):3736–3745
- Elad M, Matalon B, Zibulevsky M (2006b) Image denoising with shrinkage and redundant representations. In: *IEEE computer society conference on computer vision and pattern recognition*, vol 2, pp 1924–1931
- Gross RS (2000) The excitation of the Chandler wobble. *Geophys Res Lett* 27(15):2329–2332
- Gross RS, Fukumori I, Menemenlis D (2003) Atmospheric and oceanic excitation of the Earth's wobbles during 1980–2000. *J Geophys Res*. doi:10.1029/2002JB002143
- Guo JY, Greiner-Mai H, Ballani L, Jochmann H, Shum CK (2005) On the double-peak spectrum of the Chandler wobble. *J Geodesy* 78(11–12):654–659
- Harris FJ (1978) On the use of windows for harmonic analysis with the discrete Fourier transform. *Proc IEEE* 66(1):51–83
- Höpfner J (2000) The international latitude service—a historical review, from the beginning to its foundation in 1899 and the period until 1922. *Surv Geophys* 21(5–6):521–566
- Höpfner J (2003a) Polar motions with a half-Chandler period and less in their temporal variability. *J Geodyn* 36(3):407–422

- Höpfner J (2003b) Chandler and annual wobbles based on space-geodetic measurements. *J Geodyn* 36(3):369–381
- Höpfner J (2004) Low-frequency variations, Chandler and annual wobbles of polar motion as observed over one century. *Surv Geophys* 25(1):1–54
- Huang K, Aviyente S (2006) Sparse representation for signal classification. In: advances in neural information processing systems, pp 609–616
- IERS (1999) 1998 Annual report, Obs de Paris
- Jochmann H (2003) Period variations of the Chandler wobble. *J Geodesy* 77(7–8):454–458
- King NE, Agnew DC (1991) How large is the retrograde annual wobble? *Geophys Res Lett* 18(9):1735–1738
- Klimov DM, Akulenko LD, Kumakshev SA (2014) The main properties and peculiarities of the Earth's motion relative to the center of mass. In: *Doklady physics*, vol 59(10). Pleiades Publishing, pp 472–475
- Kosek W (1995) Time variable band pass filter spectra of real and complex-valued polar motion series. *Artif Satell* 24:27–43
- Kuehne J, Wilson CR (1991) Terrestrial water storage and polar motion. *J Geophys Res Solid Earth* 96(B3):4337–4345
- Kuehne J, Wilson CR, Johnson S (1996) Estimates of the Chandler wobble frequency and Q. *J Geophys Res Solid Earth* 101(B6):13573–13579
- Lambeck K (2005) The Earth's variable rotation: geophysical causes and consequences. Cambridge University Press, New York
- Lenhardt H, Groten E (1985) Chandler wobble parameters from BIH and ILS data. *Manuscr Geod* 10:296–305
- Li Y, Cichocki A, Amari SI (2004) Analysis of sparse representation and blind source separation. *Neural Comput* 16(6):1193–1234
- Liu L, Hsu H, Grafarend EW (2007) Normal Morlet wavelet transform and its application to the Earth's polar motion. *J Geophys Res*. doi:[10.1029/2006JB004895](https://doi.org/10.1029/2006JB004895)
- Malkin Z, Miller N (2010) Chandler wobble: two more large phase jumps revealed. *Earth Planets Space* 62(12):943–947
- Mallat S (1999) A wavelet tour of signal processing. Academic Press, California
- Mallat SG, Zhang Z (1993) Matching pursuits with time-frequency dictionaries. *IEEE Trans Signal Process* 41(12):3397–3415
- Mann S, Haykin S (1992) Adaptive chirplet transform: an adaptive generalization of the wavelet transform. *Opt Eng* 31(6):1243–1256
- Melchior PJ (1954) Contribution a l'etude des mouvements de l'axe instantane de rotation par rapport AU globe terrestre. Ixelles, Impr. R. Louis, 1954, 1
- Melchior PJ (1957) Latitude variation. *Progress Phys Chem Earth* 2:212–243
- Merriam JB (1982) Meteorological excitation of the annual polar motion. *Geophys J Int* 70(1):41–56
- Mihovilović D, Bracewell RN (1991) Adaptive chirplet representation of signals on time–frequency plane. *Electron Lett* 27(13):1159–1161
- Munk W (1961) Atmospheric excitation of the Earth's wobble. *Geophys J Int* 4(Supplement 1):339–358
- Nastula J, Ponte RM (1999) Further evidence for oceanic excitation of polar motion. *Geophys J Int* 139(1):123–130
- Okubo S (1982) Is the Chandler period variable? *Geophys J Int* 71(3):629–646
- Olshausen BA, Sallee P, Lewicki MS (2001) Learning sparse image codes using a wavelet pyramid architecture. In: Leen TK, Dietterich TG, Tresp V (eds) *Advance in neural information processing system* 13. MIT Press, Cambridge, pp 887–893
- Pati YC, Rezaifar R, Krishnaprasad PS (1993) Orthogonal matching pursuit: recursive function approximation with applications to wavelet decomposition. In: *signals, systems and computers, 1993*. 1993 conference record of The twenty-seventh Asilomar conference, pp 40–44
- Popiński W, Kosek W (1995) The Fourier transform band pass filter and its application for polar motion analysis. *Artif Satell Planet Geodesy* (no. 24) 30(1):9–25
- Rubinstein R, Bruckstein AM, Elad M (2010) Dictionaries for sparse representation modeling. *Proc IEEE* 98(6):1045–1057
- Salstein D (2000) Atmospheric excitation of polar motion. In: *IAU Colloq. 178: Polar motion: historical and scientific problems*, vol 208. p 437
- Schuh H, Nagel S, Seitz T (2001) Linear drift and periodic variations observed in long time series of polar motion. *J Geodesy* 74(10):701–710
- Sekiguchi N (1972) On some properties of the excitation and damping of the polar motion. *Publ Astron Soc Jpn* 24:99

- Sekiguchi N (1976) An interpretation of the multiple-peak spectra of the polar wobble of the Earth. *Publ Astron Soc Jpn* 28:277–291
- Smylie DE, Henderson GA, Zuberi M (2015) Modern observations of the effect of earthquakes on the Chandler wobble. *J Geodyn* 83:85–91
- Starck JL, Elad M, Donoho DL (2005) Image decomposition via the combination of sparse representations and a variational approach. *IEEE Trans Image Process* 14(10):1570–1582
- Tary JB, Herrera RH, Han J, Baan M (2014) Spectral estimation—what is new? What is next? *Rev Geophys* 52(4):723–749
- Vicente RO, Wilson CR (1997) On the variability of the Chandler frequency. *J Geophys Res Solid Earth* 102(B9):20439–20445
- Wahr JM (1982) The effects of the atmosphere and oceans on the Earth's wobble—I Theory. *Geophys J Int* 70(2):349–372
- Wahr JM (1983) The effects of the atmosphere and oceans on the Earth's wobble and on the seasonal variations in the length of day—II. Results. *Geophys J Int* 74(2):451–487
- Wilson CR, Haubrich RA (1976) Meteorological excitation of the Earth's wobble. *Geophys J Int* 46(3):707–743
- Wilson CR, Vicente RO (1990) Maximum likelihood estimates of polar motion parameters. In: McCarthy DD, Carter WE (eds) *Variations in earth rotation*. American Geophysical Union, pp 151–155
- Zhong M, Naito I, Kitoh A (2003) Atmospheric, hydrological, and ocean current contributions to Earth's annual wobble and length-of-day signals based on output from a climate model. *J Geophys Res*. doi:[10.1029/2001JB000457](https://doi.org/10.1029/2001JB000457)
- Zotov LV, Bizouard C (2015) Regional atmospheric influence on the Chandler wobble. *Adv Space Res* 55(5):1300–1306